Rationally designed bicyclic peptides prevent the conversion of Aβ42 assemblies into fibrillar structures

Tatsuya Ikenoue[1], Francesco A. Aprile[1,2], Pietro Sormanni[1], Michele Vendruscolo[1]

[1]*Centre for Misfolding Diseases, Department of Chemistry, University of Cambridge, Cambridge CB2 1EW, UK*

[2]*Department of Chemistry, Molecular Sciences Research Hub, Imperial College London, London W12 0BZ, UK*

Abstract

There is great interest in drug discovery programs targeted at the aggregation of the 42-residue form of the amyloid β peptide (Aβ42), since this molecular process is closely associated with Alzheimer's disease. The use of bicyclic peptides may offer novel opportunities for the effective modification on Aβ42 aggregation and inhibition of its cytotoxicity, as these compounds combine the molecular recognition ability of antibodies with a relatively small size of about 2 kD. Here, to pursue this approach, we rationally designed a panel of six bicyclic peptides targeting various epitopes along the sequence of Aβ42 to scan its most amyloidogenic region (residues 13-42). Our kinetic analysis and structural studies revealed that at sub-stoichiometric concentrations the designed bicyclic peptides induce a delay in the condensation of Aβ42 and the subsequent transition to a fibrillar state, while at higher concentrations they inhibit such transition. We thus suggest that designed bicyclic peptides can be employed to inhibit amyloid formation by redirecting the aggregation process towards amorphous assemblies.

Introduction

Since the formation of aberrant deposits composed primarily of the amyloid β peptide (Aβ) is a molecular hallmark of Alzheimer's disease[1,2], a major therapeutic strategy for this condition has been based on the discovery of compounds capable of inhibiting Aβ aggregation[3,4]. However, disease-modifying compounds have not yet become available[5]. Major drug discovery efforts have been devoted to the identification of small molecules, which have high brain penetration and low manufacturing costs, but also typically low specificity and high risk of side effects. In parallel, other efforts have been devoted to the development of antibodies, which have the advantage of high specificity, but the disadvantages of high manufacturing costs, difficulty for administration, low permeability and sometimes poor developability[6].

Bicyclic peptides have recently been introduced in the drug discovery field as they are thought to enable the combination of the advantages of small molecules with those of antibodies[7-13]. These compounds consist of polypeptide chains where three cysteine residues spaced within the sequence are chemically linked to a cyclic compound. This design results in the formation of two macrocyclic rings that serve as binding regions (**Fig. 1**). As the topology of bicyclic peptides is restrained they have a relatively small entropy cost upon binding and thus a good binding affinity and specificity[11,13,14]. Having a small size of about 2 kDa, at least in principle, they are endowed with multiple advantages over antibodies, including the possibility of simple chemical synthesis, better tissue penetration, higher resistance to protease cleavage and inactivation, and extended half-life *in vivo*[15].

Bicyclic peptides against specific targets can be developed in a variety of ways. Phage display, for example, can be used for the isolation of these compounds from large combinatorial libraries[13,16,17]. This method, however, may become time-consuming and at times ineffective, in particular when

one aims at targeting aggregation-prone antigens or weakly immunogenic epitopes. To overcome these limitations, we have introduced a method for the rationally design of antibodies[6,18-20] and bicyclic peptides[21], which enables the targeting of specific epitopes within intrinsically disordered proteins.

Here, we present an application of this design strategy by generating a panel of bicyclic peptides capable of binding Aβ42 and interfering with its aggregation process. Aβ42 aggregates through a complex process that involves the combination of different microscopic steps and multiple molecular species[22,23]. In this context, it is becoming increasingly recognised that the Aβ42 oligomers formed during the aggregation process are highly neurotoxic[24,25]. Therefore, therapeutic strategies are being developed to decrease the concentrations of these oligomeric species, for example by delaying or preventing their formation[19,22,24,26-30]. In one of such strategy, the amyloid aggregation process is redirected towards off-pathway non-toxic species. The small molecule trodusquemine, for example, can modulate the aggregation process of Aβ42 and by redirecting it towards the formation of off-pathway non-toxic aggregates[31]. Furthermore, strategies aimed at reducing the populations of oligomers by speeding up the aggregation process have also been proposed[32-34]. Along these lines, we show here that our rationally designed bicyclic peptides prevent the conversion of Aβ42 assemblies into fibrillar structure.

Results

Rational design and synthesis of bicyclic peptides targeting different Aβ42 epitopes

We employed the cascade method, a computational antibody discovery strategy[6,18,21], to generate six bicyclic peptides targeting different regions of the amino acid sequence of Aβ42 (**Methods)**. These six peptides (DesBP1 to DesBP6) were designed to scan epitopes in the most amyloidogenic

region of Aβ42 (residues 13-42) (**Fig. 1a**) (**Methods)**. For the cyclisation, we incorporated in the designed sequences three cysteine residues separated by two groups of six residues (**Fig. 1a**). Because the cyclisation achieved via reducible disulfide bonds could be problematic for therapeutic purposes, we then used tris-(bromomethyl)benzene (TBMB), a small bromine-containing organic compound, as a scaffold to anchor each designed peptide (**Fig. 1b**). We carried out the reaction in aqueous solvents at 30 °C in 1 h, with the three-fold rotational symmetry of the TBMB molecule ensuring the formation of a unique structural and spatial isomer. The synthesized bicyclic peptides showed high purity (> 95%). To assess the solubility of the DesBPs in phosphate buffer, static and dynamic light scattering (DLS) measurements were performed immediately after ultracentrifugation (**Fig. S1a,b**). The results showed 50 μM of all the DesBPs remained largely soluble at 5 °C, except DesBP4, which formed assemblies of about ~140 nm in size (**Fig. S1d**). Far-UV CD spectra show that DesBP1, DesBP2, DesBP5, and DesBP6 tend to retain structured states (**Fig. S1c**). AFM images taken after one day, however, showed the presence of assemblies in all cases (**Fig. S1d**).

Characterisation of the effects of the DesBPs on the aggregation kinetics of Aβ42

In order to investigate the effects of the DesBPs on Aβ42 aggregation, we carried out *in vitro* aggregation assays using the fluorescent dye thioflavin T (ThT) as amyloid-sensitive probe. We monitored Aβ42 fibril formation at the concentration of 2 μM in the presence of different molar ratios [Aβ42]:[DesBP] (from 0.05 to 16) at 37 °C under quiescent conditions, using a highly reproducible aggregation assay previously described[21,35].

Sub-stoichiometric concentrations of DesBPs delay Aβ42 aggregation and increase ThT fluorescence. In the presence of low concentrations of DesBPs, we observed significant changes in the ThT fluorescence intensities in the presence of DesBP1, DesBP2, DesBP5 and DesBP6, both in unseeded (**Fig. 2a-c**) and in seeded assays (**Fig. S2**), but not in the presence of DesBP3 and

DesBP4 (**Fig. S3**), a result likely due to the presence of the solubilizing DED motif on DesBP3 and DesBP4. The DED motif generates an electrostatic repulsion with the ED motif on Aβ42, which is likely to interfere with the designed epitope-paratope complementarity (**Fig. 1a**). From the analysis of the normalized curves (**Fig. 2b**), we obtained the dependence of the half-time of aggregation ($t_{1/2}$) on the concentrations of the DesBPs, which indicate that these bicyclic peptides delay the aggregation process of Aβ42 (**Fig. 2c**).

High concentrations of DesBPs delay Aβ42 aggregation and decrease ThT fluorescence. We then tested the effects of high concentrations (0.25- to 16-fold excess) of the DesBPs on the Aβ42 aggregation process (**Fig. 3**). The ThT profiles of DesBP1, DesBP2, DesBP5 and DesBP6 (**Fig. 3a**), but again not of DesBP3 and DesBP4 (**Fig. S3**), showed an increase in $t_{1/2}$ (**Fig. 3b**). At the same time, we observed a suppression of the ThT intensity (**Fig. 3c**) as the concentrations of the DesBPs were increased. To investigate this phenomenon, we studied the morphological changes of the aggregates by using the fluorescent probe ANS, which binds to hydrophobic surfaces. The comparison of the ThT and ANS profiles is shown in **Fig. 3c,** and individual ThT and ANS fluorescence profiles at various concentrations of DesBPs are shown in **Fig. S4**. We observed that the ANS intensity was increased in a concentration-dependent manner, while the ThT intensity was suppressed (**Figs. 3c** and **S4**), indicating that the DesBPs induced structural changes to more hydrophobic aggregates.

To further characterize the morphology of the aggregates, we used atomic force microscopy (AFM) after each incubation in the absence and in the presence of 0.25 and 16 molar equivalents of the DesBPs (**Fig. 3d**). Representative AFM images show a morphological transition from fibrillar to non-fibrillar aggregates, consistent with the increase of ANS fluorescence. These different morphologies are presumably caused by the incorporation of the DesBPs into the Aβ42 aggregates. Furthermore, the aggregates did not show seeding ability, apart from those formed in the presence

of DesBP6, suggesting that they are not fibrillar (**Fig. S5**).

Taken together, our results indicate that these DesBPs extend the lag phase at all concentrations, but appear to exhibit a concentration-dependent mechanism of modulation of Aβ42 aggregation. At low concentrations, the DesBPs increase the ThT intensity (**Fig. 2**), while at higher concentrations they decrease the ThT intensity by redirecting the aggregation process towards non-fibrillar aggregates (**Fig. 3**).

Characterisation of the effects of the DesBPs on the structures of the aggregates of Aβ42

Sub-stoichiometric concentrations of DesBPs delay the aggregation of Aβ42 into fibrillar structures. To investigate the structures of the Aβ42 aggregates formed in the presence of the DesBPs, we performed time course dynamic light scattering (DLS) measurements to monitor the early stages of aggregation of 10 μM Aβ42 in the presence of 0.25 molar equivalents of DesBP (**Fig. 4a**). The results showed a rapid (within 10 minutes) appearance of aggregates of about 1.0 μm in size. The ThT profiles, however, did not show any increase until at least 30 min (**Fig. 4b**), showing that these early aggregates do not yet have a fully-ordered fibrillar structure. In addition, the growth in the ANS signal within the initial 30 min suggests the presence of hydrophobic assemblies (**Fig. 4b**). Next, in the presence of 0.25 molar equivalents of the DesBPs, the Aβ42 concentration was varied from 2 to 10 μM in the ThT assays. To confirm that the products were still amyloid fibrils, far-UV CD spectrometry measurements were performed in the case of 10 μM of Aβ42. After a 1-day incubation, the CD spectra showed fibrillar structures, although aggregates in the presence of DesBP2 and DesBP5 showed less β-sheet contents (**Fig. 4e**). The ThT profiles indicate that the aggregation of Aβ42 was enhanced in the presence of the DesBPs (**Fig. 4f**), without the formation of significant amounts of off-pathway aggregates (**Fig. S6**). We then evaluated the

changes the half-time of aggregation, finding that the $t_{1/2}$ values in the presence of DesBP1, DesBP2, DesBP5, and DesBP6 were increased in a concentration-dependent manner (**Fig. 4g**).

High concentrations of DesBPs delay Aβ42 aggregation and promote the formation of amorphous assemblies. In the presence of 16-fold excess DesBP concentration, for 2 μM Aβ42 concentration, the analysis of DLS (**Fig. 4c**), ThT and ANS (**Fig. 4d**) measurements indicated a gradual formation of amorphous assemblies, presumably of mixed Aβ42/DesBP composition, since the intensity of the ThT and ANS decreases by about 20-fold at high DesBP concentration. At high DesBP concentrations the aggregates appear to be no longer fibrillar, as also shown by the AFM images in **Fig. 3** and the seeding experiments in **Fig. S5**.

Taken together, these results show that DesBPs promote the condensation of Aβ42 monomers into assemblies formed by interacting Aβ42 and DesBP molecules in the early stages of Aβ42 aggregation. The presence of these assemblies delays, or even blocks, the formation of structured aggregates in the late stages.

Conclusions

We have described the effects on the aggregation process of Aβ42 of a panel of bicyclic peptides designed to bind different epitopes along the Aβ42 sequence. Our results show that in the early phases of aggregation there is a condensation of mixed assemblies formed by the Aβ42 and DesBP molecules (**Fig. 5**). In the late phases, at low DesBP concentrations these assemblies tend to convert into fibrillar structures, while at high DesBP concentrations they mature into amorphous aggregates (**Fig. 5**). These results indicate that bicyclic peptides can be used to remodel the Aβ42 aggregation process by redirecting it towards non-fibrillar species.

Materials and Methods

Reagents

All reagents were purchased from Sigma Aldrich, excluding thioflavin T UltraPure Grade (ThT ≥ 95%), which was purchased from Eurogentec Ltd.

Rational design of the bicyclic peptides

In our rational design strategy, we regard a bicyclic peptide sequence as formed by four regions, which are separated by the three cysteine residues required for bicyclisation. In this view, we designed the two central regions to enable the binding to the target epitope, as depicted in **Fig. 1b**. By contrast, we retained some motifs (i.e. Ala-Ala at the N-terminus and Gly-Gly at the C-terminus for DesBP1, DesBP2, DesBP5 and DesBP6) of the amino acid sequences of the two terminal regions in order to facilitate the bicyclisation reaction. These regions were further endowed with charged residues to enhance the overall solubility of the constructs. We set the length of the binding sites to six or seven residues, following unsuccessful preliminary attempts to carry out the bicyclisation reaction with longer sequences, or without the Ala-Ala and Gly-Gly motifs at the termini. The rational designed was performed with the cascade method[18] (**Fig. 1a**). The charged residues at the termini were chosen using the CamSol intrinsic solubility score[36].

Recombinant expression of Aβ42

Aβ42 peptides (MDAEFRHDSGY EVHHQKLVFF AEDVGSNKGA IIGLMVGGVV IA), here called Aβ42, were obtained as described previously by recombinant expression in the *E. coli* BL21 Gold (DE3) strain (Stratagene)[37]. The purification procedure was carried out by sonication of *E. coli* cells, dissolution of inclusion bodies in 8 M urea, ion exchange in batch mode on diethylaminoethyl cellulose resin, and lyophilization, followed by further purification using a Superdex 75 HR 26/60 column (GE Healthcare). Eluates were analyzed using SDS–

polyacrylamide gel electrophoresis (SDS-PAGE) for the presence of protein products. The fractions containing recombinant Aβ42 were combined, frozen using liquid nitrogen, and lyophilized again.

Synthesis of the byciclic peptides

The rationally designed linear peptides were purchased from ChinaPeptides. In order to achieve cyclization, the peptides were dissolved in the reaction buffer (20 mM NH4HCO3, 5 mM EDTA, pH 8.0) at 625 μM. One quarter volume of 5 mM TBMB in 100% acetonitrile was added to obtain a final concentration of 500 μM peptide and 1 mM TBMB and incubated for 1 h at 30 °C. The cyclized peptides were purified by reversed-phase chromatography on a C18 column using H2O/0.08% trifluoroacetic acid (TFA) and acetonitrile/0.08% TFA as solvents, using a GRACE VYDAC C18 (218TP) column 22 × 250 mm. The correct mass was then validated by analytical LC/MS (Xevo).

ThT and ANS fluorescence aggregation assay

Solutions of monomeric peptides were prepared by dissolving the lyophilized Aβ42 peptide in 6 M GuHCl. The designed bicyclic peptides in their monomeric form were purified from oligomeric species and salt using a Superdex 75 10/300 GL column (GE Healthcare) at a flow rate of 0.5 ml/min, followed by elution in 20 mM sodium phosphate buffer (pH 8) and addition of 200 μM EDTA. The peptide concentration was determined from the absorbance of the integrated peak area using ε280 = 1495l mol^{-1} cm^{-1}. The designed bicyclic peptides were dissolved in water and centrifuged at 20 °C for 1 h at 435,000 g before use. The obtained DesAbs in their monomeric forms were diluted with buffer to the desired concentration and supplemented with 20 μM ThT and 50 μM ANS from a 1 mM stock. ANS experiments were carried out as described previously[21]. Seeding experiments were performed in the presence of 10% (v/v) preformed fibrils, as described previously[21]. Preformed fibrils were prepared by the same procedure used with spontaneous fibril formation. All samples were prepared in low-binding Eppendorf tubes on ice using careful pipetting

to avoid introduction of air bubbles. Each sample was then pipetted into multiple wells of a 96-well half-area, low-binding polyethylene glycol coating plate (Corning 3881) with a clear bottom, at 80 µl per well. Assays were initiated by placing the 96-well plate at 37 °C under quiescent conditions in a plate reader (Fluostar Optima; BMG Labtech). The fluorescence was simultaneously measured through the bottom of the plate with excitation filter at 440 nm for ThT and 380 nm for ANS and emission filter at 480 nm.

Static and dynamic light scattering

The light scattering measurements were performed on a Zetasizer Nano S instrument (Malvern Instruments, Malvern, UK) in backscattering mode at 173°. The instrument was equipped with a light source with a wavelength of 633 nm and a Peltier temperature controller at 25 °C. Samples were prepared as described above, and 70 µl of them were pipetted into disposal plastic micro cuvette.

CD spectroscopy

Far-UV CD spectra of proteins and peptides in soluble and insoluble states were measured with a J-820 spectropolarimeter (Jasco, Japan) using a cell with a light path of 1 mm at each condition. Individual Aβ42 solutions were prepared at 10 µM for CD measurements. The CD signals between 195 and 250 nm were expressed as mean residue ellipticity [θ] (deg cm^2 $dmol^{-1}$). Temperature regulation was carried out using a PFD-425S Peltier-unit (Jasco, Japan).

Atomic force microscopy

AFM measurements were carried out in air with the sample deposited on functionalized mica. To functionalize the surface, after cleaving, the bare mica substrate was incubated with a 10 µl drop of 0.05% (v/v) APTES ((3-Aminopropyl)triethoxysilane, Fluka) in Milli-Q water for 1 min at room temperature, rinsed with Milli-Q water and then dried by the passage of a gentle flow of gaseous

nitrogen. The preparation of the mica AFM samples was made at room temperature by deposition of a 10 µl aliquot of 10 µM solution for 5 min. Then the samples were rinsed with ultrapure water and dried by a gentle flow of nitrogen.

AFM imaging was carried out in intermittent contact mode on a JPK Nanowizard II atomic force microscope (AFM) recorded with AC mode under ambient conditions using an integral gain of 120 Hz, post-gain of 0.008 Hz, 0.3 Hz line-rate for 4 by 4 µm images. Images flattening and statistical analysis was performed by SPIP (Image metrology) software.

Author Contributions

T.I., F.A.A., P.S. and M.V. were involved in the design of research. P.S. designed the peptide and T.I. performed the experiments. T.I, F.A.A. and M.V. wrote the paper. All authors discussed the results and commented on the manuscript.

Funding

This work was supported by the Japan Society for the Promotion of Science (JSPS) oversea research fellowships. Francesco A. Aprile is supported by UK Research and Innovation (MR/S033947/1) and the Alzheimer's Society, UK (317, 511).

References

1 Jack Jr, C. R. *et al.* NIA-AA research framework: Toward a biological definition of Alzheimer's disease. *Alzheimer's Dementia* **14**, 535-562, (2018).

2 Selkoe, D. J. & Hardy, J. The amyloid hypothesis of Alzheimer's disease at 25 years. *EMBO Mol Med* **8**, 595-608, (2016).

3 Schenk, D. *et al.* Immunization with amyloid-beta attenuates Alzheimer-disease-like pathology in the pdapp mouse. *Nature* **400**, 173-177, (1999).

4 Sevigny, J. *et al.* The antibody aducanumab reduces Aβ plaques in Alzheimer's disease. *Nature* **537**, 50, (2016).

5 Cummings, J., Lee, G., Ritter, A., Sabbagh, M. & Zhong, K. Alzheimer's disease drug development pipeline: 2020. *Alzheimer's Dementia* **6**, e12050, (2020).

6 Sormanni, P., Aprile, F. A. & Vendruscolo, M. Third generation antibody discovery methods: In silico rational design. *Chem. Soc. Rev.* **47**, 9137-9157, (2018).

7 Driggers, E. M., Hale, S. P., Lee, J. & Terrett, N. K. The exploration of macrocycles for drug discovery--an underexploited structural class. *Nat Rev Drug Discov* **7**, 608-624, (2008).

8 Quartararo, J. S. *et al.* A bicyclic peptide scaffold promotes phosphotyrosine mimicry and cellular uptake. *Bioorg Med Chem* **22**, 6387-6391, (2014).

9 Bartoloni, M. *et al.* Bridged bicyclic peptides as potential drug scaffolds: Synthesis, structure, protein binding and stability. *Chem. Sci.* **6**, 5473-5490, (2015).

10 Getz, J. A., Rice, J. J. & Daugherty, P. S. Protease-resistant peptide ligands from a knottin scaffold library. *ACS Chem Biol* **6**, 837-844, (2011).

11 Bionda, N. & Fasan, R. Ribosomal synthesis of natural-product-like bicyclic peptides in escherichia coli. *Chembiochem* **16**, 2011-2016, (2015).

12 Lian, W., Jiang, B., Qian, Z. & Pei, D. Cell-permeable bicyclic peptide inhibitors against

intracellular proteins. *J Am Chem Soc* **136**, 9830-9833, (2014).

13 Angelini, A. *et al.* Bicyclic peptide inhibitor reveals large contact interface with a protease target. *ACS Chem Biol* **7**, 817-821, (2012).

14 Chen, S., Bertoldo, D., Angelini, A., Pojer, F. & Heinis, C. Peptide ligands stabilized by small molecules. *Angew Chem Int Ed Engl* **53**, 1602-1606, (2014).

15 Bock, J. E., Gavenonis, J. & Kritzer, J. A. Getting in shape: Controlling peptide bioactivity and bioavailability using conformational constraints. *ACS Chem Biol* **8**, 488-499, (2013).

16 Heinis, C., Rutherford, T., Freund, S. & Winter, G. Phage-encoded combinatorial chemical libraries based on bicyclic peptides. *Nat Chem Biol* **5**, 502-507, (2009).

17 Baeriswyl, V. & Heinis, C. Polycyclic peptide therapeutics. *ChemMedChem* **8**, 377-384, (2013).

18 Sormanni, P., Aprile, F. A. & Vendruscolo, M. Rational design of antibodies targeting specific epitopes within intrinsically disordered proteins. *Proc Natl Acad Sci U S A* **112**, 9902-9907, (2015).

19 Aprile, F. A. *et al.* Selective targeting of primary and secondary nucleation pathways in abeta42 aggregation using a rational antibody scanning method. *Sci Adv* **3**, e1700488, (2017).

20 Aprile, F. A., Sormanni, P. & Vendruscolo, M. A rational design strategy for the selective activity enhancement of a molecular chaperone toward a target substrate. *Biochemistry* **54**, 5103-5112, (2015).

21 Ikenoue, T. *et al.* A rationally designed bicyclic peptide remodels Aβ42 aggregation in vitro and reduces its toxicity in a worm model of Alzheimer's disease. *Scientific reports* **10**, 1-15, (2020).

22 Cohen, S. I. *et al.* Proliferation of amyloid-beta42 aggregates occurs through a secondary nucleation mechanism. *Proc Natl Acad Sci U S A* **110**, 9758-9763, (2013).

23 Michaels, T. C. *et al.* Chemical kinetics for bridging molecular mechanisms and

macroscopic measurements of amyloid fibril formation. *Annu. Rev. Phys. Chem.* **69**, 273-298, (2018).

24 Benilova, I., Karran, E. & De Strooper, B. The toxic abeta oligomer and Alzheimer's disease: An emperor in need of clothes. *Nat. Neurosci.* **15**, 349-357, (2012).

25 Mannini, B. *et al.* Toxicity of protein oligomers is rationalized by a function combining size and surface hydrophobicity. *ACS Chem Biol* **9**, 2309-2317, (2014).

26 Lesne, S. *et al.* A specific amyloid-beta protein assembly in the brain impairs memory. *Nature* **440**, 352-357, (2006).

27 Cremades, N. *et al.* Direct observation of the interconversion of normal and toxic forms of alpha-synuclein. *Cell* **149**, 1048-1059, (2012).

28 Haass, C. & Selkoe, D. J. Soluble protein oligomers in neurodegeneration: Lessons from the Alzheimer's amyloid beta-peptide. *Nat Rev Mol Cell Biol* **8**, 101-112, (2007).

29 Kayed, R. *et al.* Common structure of soluble amyloid oligomers implies common mechanism of pathogenesis. *Science* **300**, 486-489, (2003).

30 Bucciantini, M. *et al.* Inherent toxicity of aggregates implies a common mechanism for protein misfolding diseases. *Nature* **416**, 507-511, (2002).

31 Limbocker, R. *et al.* Trodusquemine enhances Aβ 42 aggregation but suppresses its toxicity by displacing oligomers from cell membranes. *Nat. Comm.* **10**, 225, (2019).

32 Sonzini, S., Stanyon, H. F. & Scherman, O. A. Decreasing amyloid toxicity through an increased rate of aggregation. *Phys Chem Chem Phys* **19**, 1458-1465, (2017).

33 Bieschke, J. *et al.* Small-molecule conversion of toxic oligomers to nontoxic beta-sheet-rich amyloid fibrils. *Nat Chem Biol* **8**, 93-101, (2011).

34 Civitelli, L. *et al.* The luminescent oligothiophene p-ftaa converts toxic abeta1-42 species into nontoxic amyloid fibers with altered properties. *J Biol Chem* **291**, 9233-9243, (2016).

35 Hellstrand, E., Boland, B., Walsh, D. M. & Linse, S. Amyloid beta-protein aggregation produces highly reproducible kinetic data and occurs by a two-phase process. *ACS Chem*

Neurosci **1**, 13-18, (2010).

36 Sormanni, P., Aprile, F. A. & Vendruscolo, M. The camsol method of rational design of protein mutants with enhanced solubility. *J Mol Biol* **427**, 478-490, (2015).

37 Habchi, J. *et al.* Systematic development of small molecules to inhibit specific microscopic steps of abeta42 aggregation in Alzheimer's disease. *Proc Natl Acad Sci U S A* **114**, E200-E208, (2017).

38 Michaels, T. C. *et al.* Dynamics of oligomer populations formed during the aggregation of Alzheimer's Aβ42 peptide. *Nat. Chem.* **12**, 445-451, (2020).

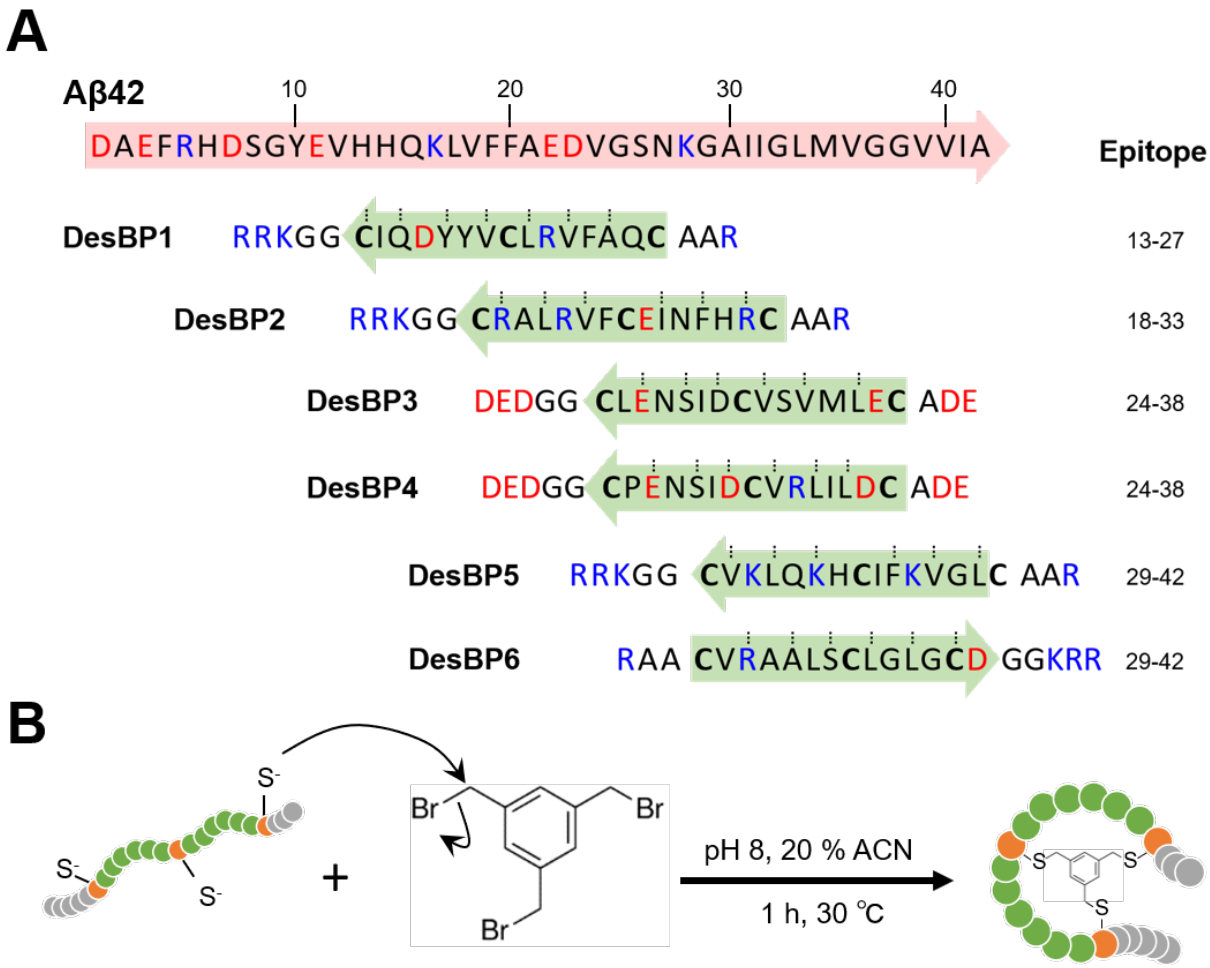

Figure 1. Generation of the rationally designed bicyclic peptides. (A) Representation of the six amino acids sequences designed to bind Aβ42 (DesBP1-DesBP6). Three cysteine residues are included for cyclization (bold) and the binding site obtained from the cascade procedure (green and blue arrows) is inserted between cysteine residues. Charged residues are added at N- and C- termini to improve solubility and modulate the binding; positive ones (blue) for DesBP1, DesBP2, DesBP5 and DesBP6, and negative ones (red) for DesBP3 and DesBP4 as controls. Dotted lines mark residues predicted to be involved in backbone-backbone hydrogen bonding and arrows denote the N- to C- termini direction. **(B)** Synthesis of the bicyclic peptides. A rationally designed peptide with three cysteine residues is tethered to the trifunctional compound 1,3,5-tris(bromomethyl)benzene (TBMB) in a nucleophilic substitution reaction.

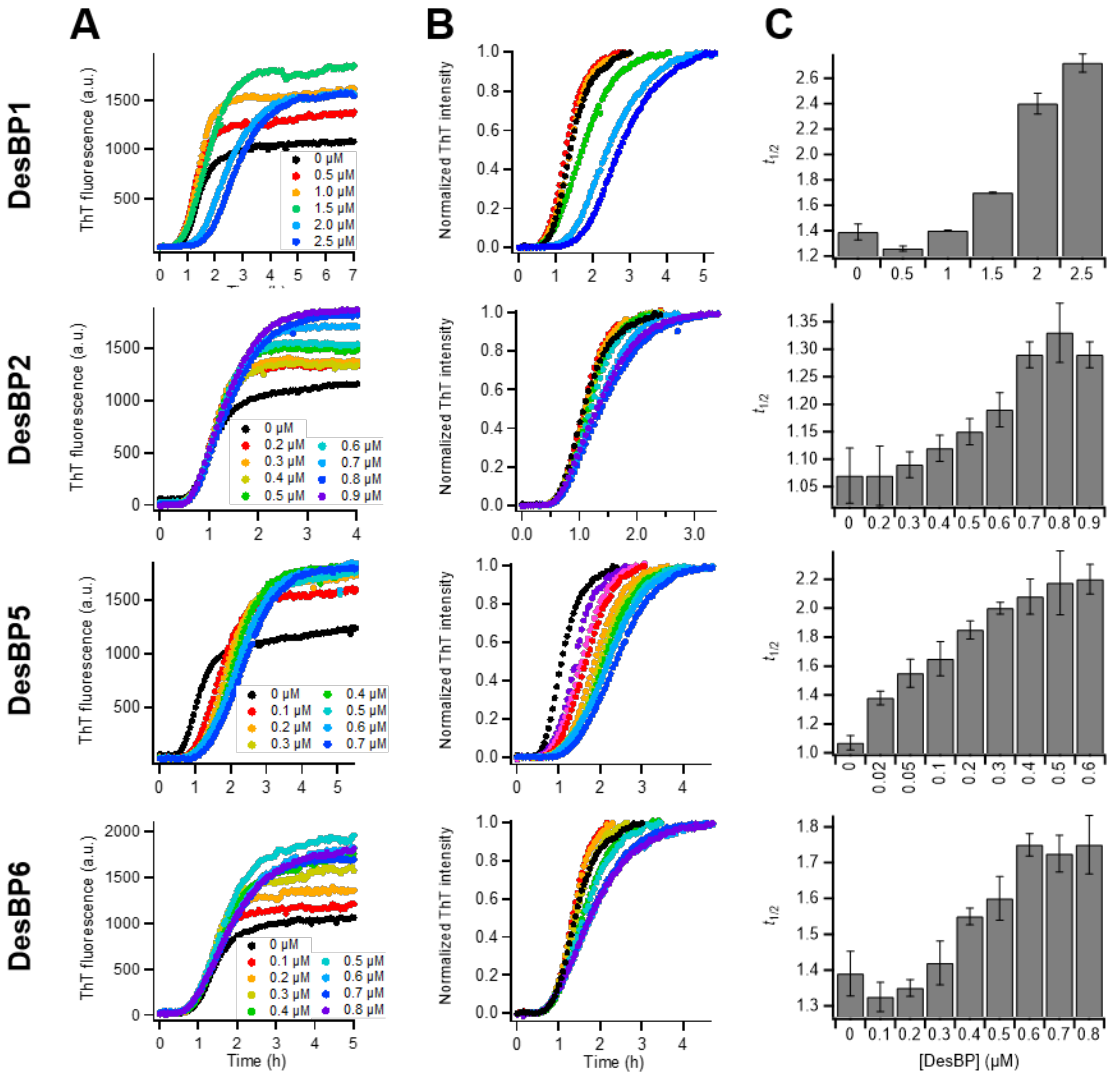

Figure 2. Kinetic analysis of Aβ42 aggregation in the presence of sub-stoichiometric concentrations of DesBPs. (A, B) Non-normalised (A) and normalized (B) ThT fluorescence intensity profiles of Aβ42 aggregation under quiescent conditions at a concentration of 2 μM in the presence of increasing concentrations (0.0-0.9 μM) of DesBPs (represented by different colors). Representative curves of three replicates are shown. **(C)** Average half-time ($t_{1/2}$) of the aggregation reaction at different [Aβ42]:[DesBP] ratios. All experiments were performed in triplicate. For reference, see Ref. [21].

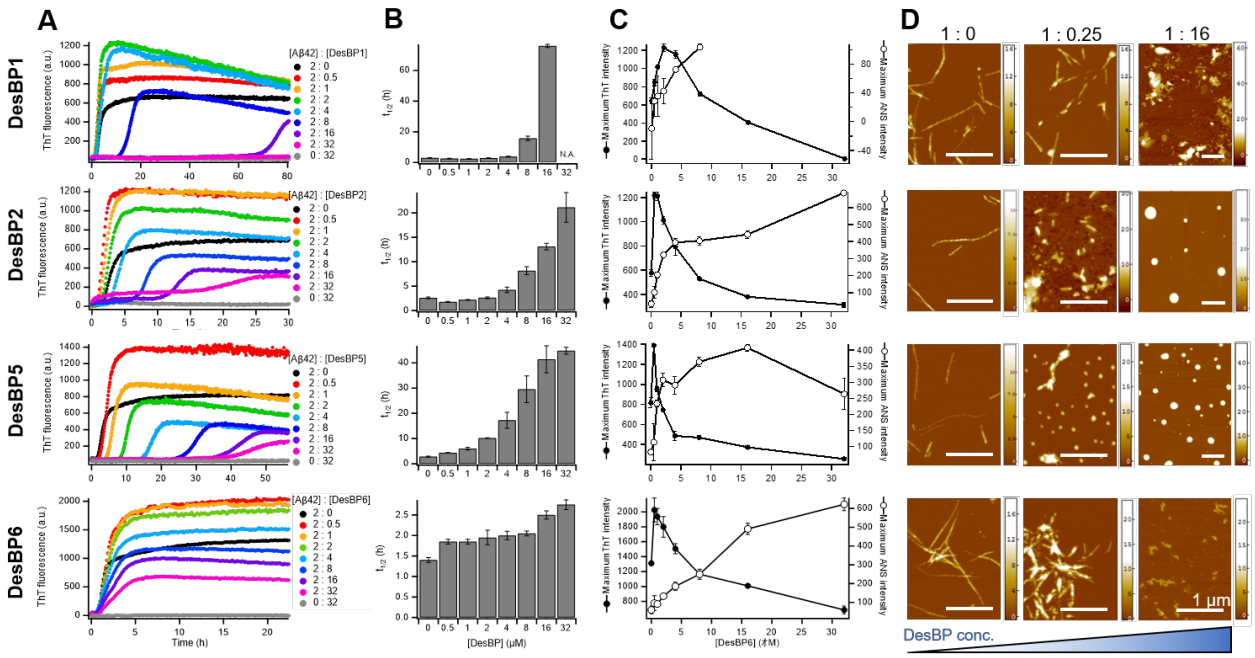

Figure 3. Kinetic analysis and morphological changes of Aβ42 aggregation in the presence of high concentrations of DesBPs. (A) ThT kinetic profiles of Aβ42 aggregation under quiescent conditions at a concentration of 2 μM in the absence or in the presence of increasing concentrations (0.5-32 μM) of DesBPs (represented by different colors). Representative profiles of three replicates are shown. **(B)** Average half-time ($t_{1/2}$) of the aggregation at each [Aβ42]:[DesBP] ratio. **(C)** Averaged maximum ThT (closed circle) and ANS (opened circle) fluorescence intensity at each [Aβ42]:[DesBP] ratio (kinetic profiles are showed in **Fig. S4**). All aggregation experiments were performed in triplicate. **(D)** Representative AFM images of Aβ42 aggregates at the end of the ThT assay (32 h) formed in the presence of 0 (left), 0.25 (middle), and 16 (right) molar equivalents of DesBPs. The scale bar on the AFM images indicates 1 μm, and the scale on the right represents the height.

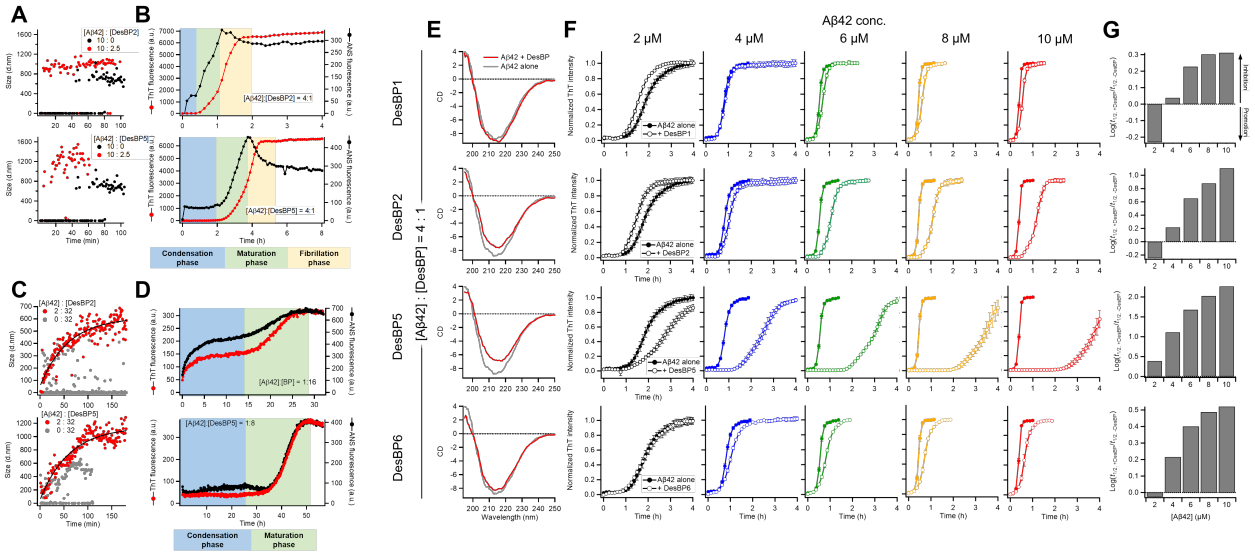

Figure 4. Comparison of the structural properties of Aβ42 aggregates at low and high DesBP concentrations. (A-D) Kinetics of 10 μM Aβ42 aggregation observed by DLS (**A,C**), ThT and ANS fluorescence (**B,D**) in the presence of 0.25 and 16 molar equivalents of DesBP2 and DesBP5. Blue, green, and yellow regions in (B) and (D) represent the condensation, maturation, and fibrillation phases in the aggregation process of Aβ42, respectively. (**E**) Secondary structure of Aβ42 aggregates in the presence of 0.25 molar equivalents DesBPs. Far-UV CD spectra of 10 μM Aβ42 aggregates in the absence (gray) and in the presence (red) of DesBPs. (**F,G**) Kinetics of Aβ42 aggregation in the presence of 0.25 molar equivalents DesBPs for increasing concentrations of Aβ42 (from 2 to 10 μM). Normalized ThT profiles (**F**) (non-normalised ThT profiles are shown in **Fig. S6**), and effects of DesBPs on $t_{1/2}$, the half time of aggregation; the y-axis reports the logarithm of the ratio of $t_{1/2}$ in the presence and absence of a DesBP (**G**). All experiments were performed in triplicate.

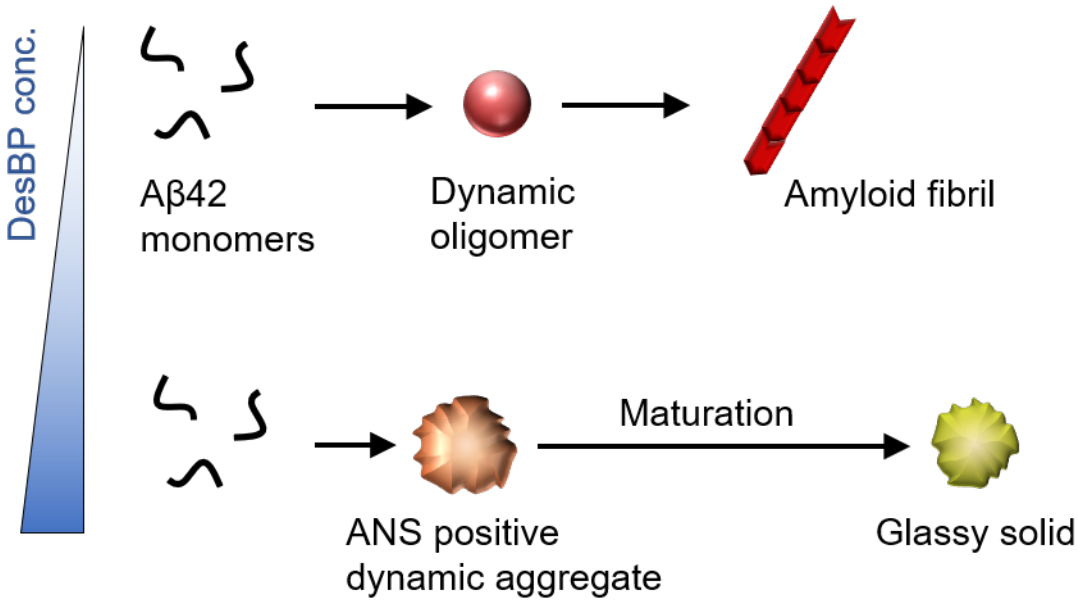

Figure 5. Effects of the DesBPs described in this work on the aggregation process of Aβ42. Our results show a condensation of mixed Aβ42/DesBP assemblies in the early phases of the aggregation process. In the late phases, at low DesBP concentrations, these assemblies are sufficiently dynamic to be able to convert into fibrillar structures, as is generally the case for Aβ42 aggregation[38], while at high DesBP concentrations they become unable to convert, and mature into amorphous aggregates.

Supplementary Information

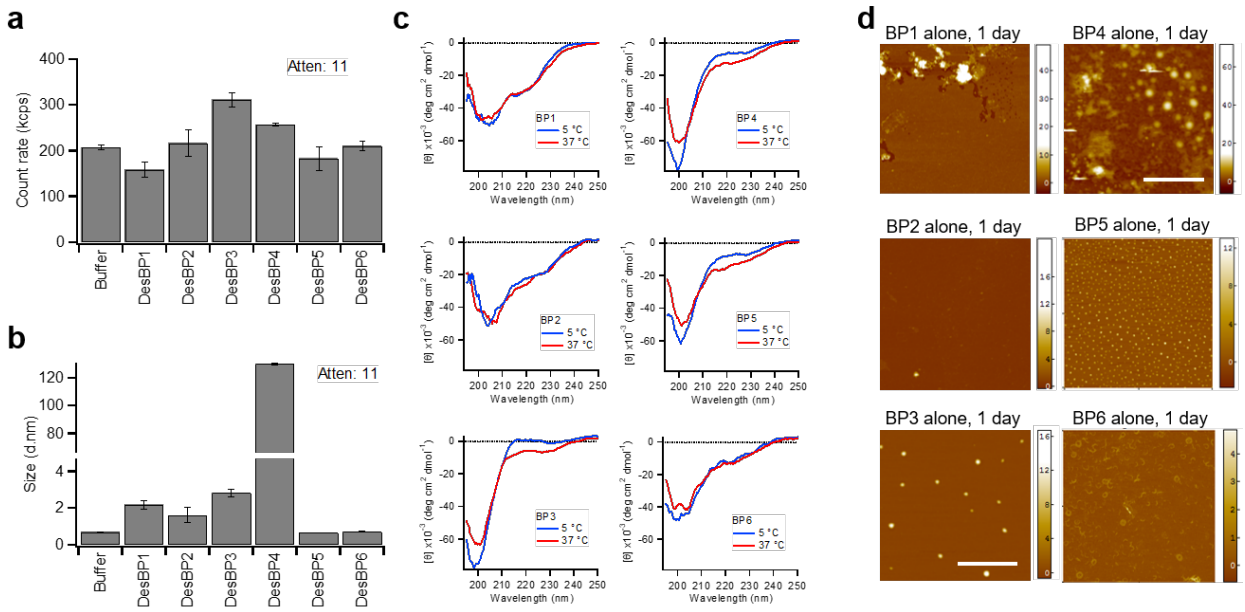

Figure S1. Solubility of the DesBPs in the absence of Aβ42 before and after incubation. (a,b) Static (a) and dynamic (b) light scattering of 50 μM DesBP monomers solved in phosphate buffer at 5 °C. **(c)** Far-UV CD spectra of 32 μM DesBP monomers. **(d)** Representative AFM images of 32 μM DesBPs after 1 day incubation at 37 °C. The scale bar on the AFM images indicates 1 μm, and the scale on the right represents the height.

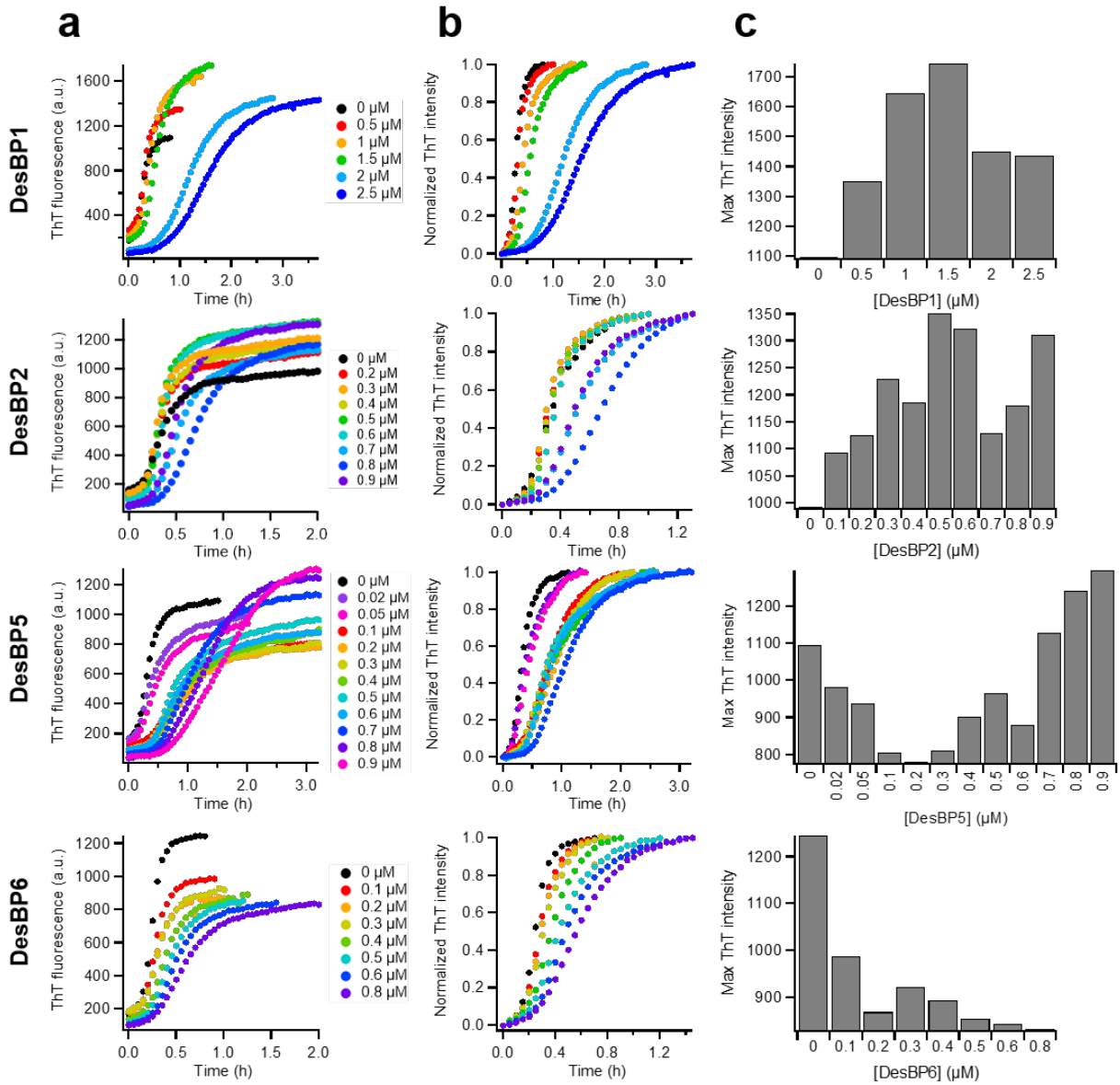

Figure S2. Seeding experiments of Aβ42 amyloid fibrils at sub-stoichiometric concentrations of DesBPs. (a,b) Non-normalised (a) and normalized ThT kinetic profiles (b) of Aβ42 aggregation under quiescent conditions at a concentration of 2 μM in the absence or in the presence of various concentrations (0.1-0.9 μM) of DesBPs (represented by different colors). **(c)** Maximum ThT intensity of the aggregation at each [Aβ42]:[DesBP] ratio. All experiments were performed in triplicate.

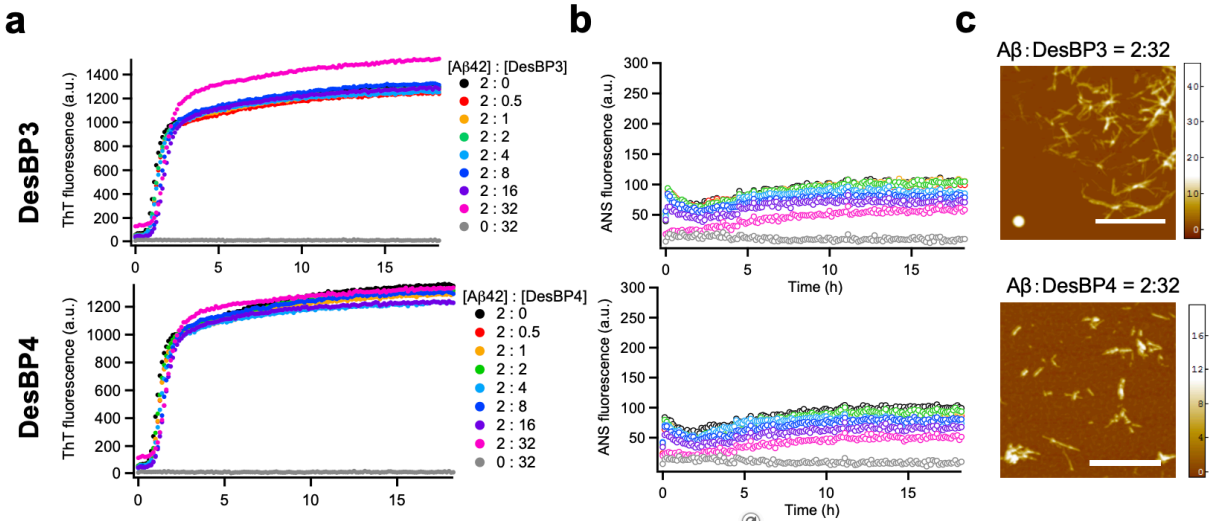

Figure S3. DesBP3 and DesBP4 do not affect significantly Aβ42 aggregation. (a,b) ThT (a) and ANS (b) kinetic profiles of Aβ42 aggregation under quiescent conditions at a concentration of 2 μM in the absence or in the presence of various concentration (0.5-32 μM) of DesBPs (represented by different colors). **(c)** Representative AFM images of Aβ42 aggregates in the presence of 16 molar equivalents of DesBPs. The scale bar on the AFM images indicate 1 μm, and the scale on the right represents the height. All aggregation experiments were performed in triplicate.

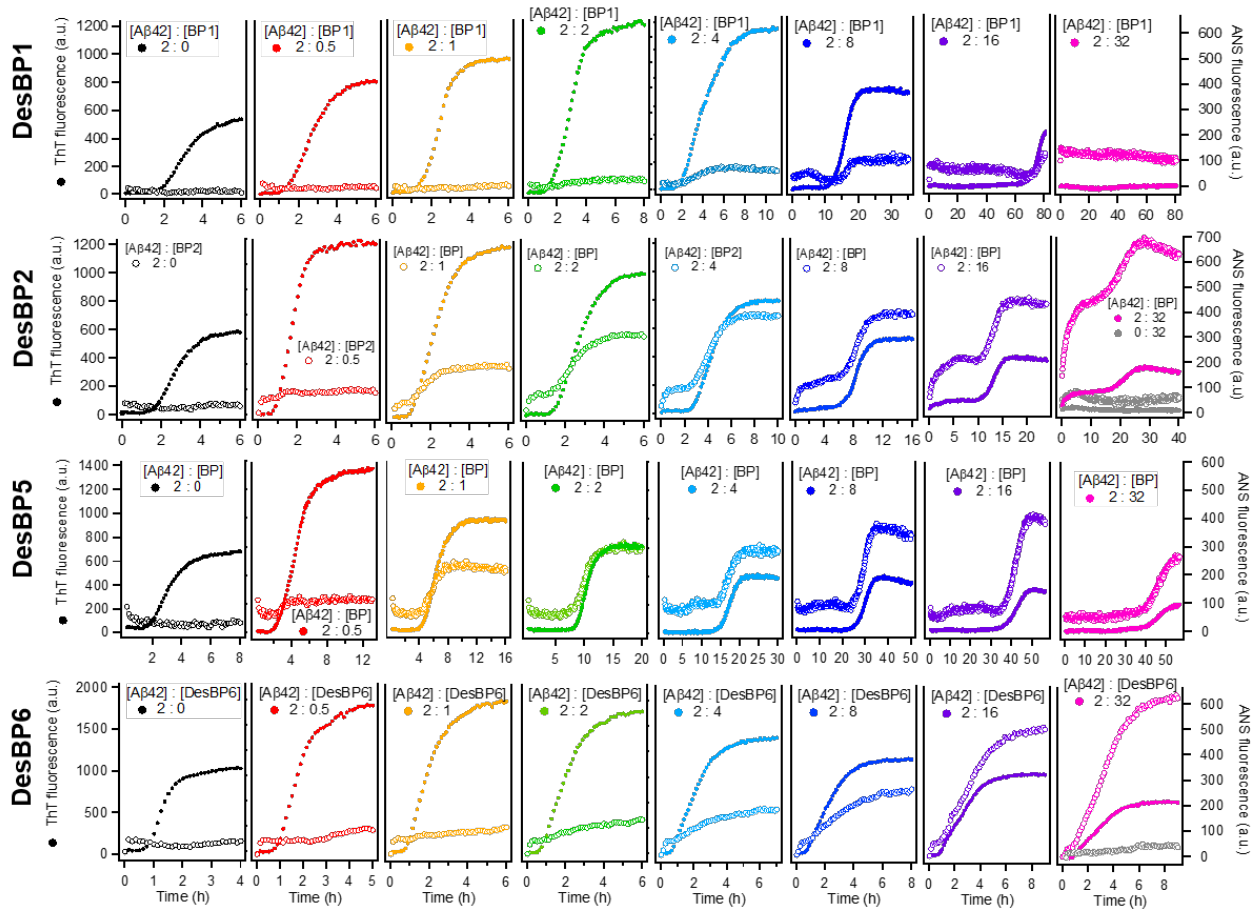

Figure S4. Kinetic profile of ThT and ANS fluorescence of Aβ42 aggregation at various concentration of DesBPs. ThT (closed circles) and ANS (opened circles) kinetic profiles of Aβ42 aggregation under quiescent conditions at a concentration of 2 μM in the absence or in the presence of various concentrations (0.5-32 μM) of DesBP1, DesBP2, DesBP5 and DesBP6 (represented by different colors). All experiments were performed in triplicate.

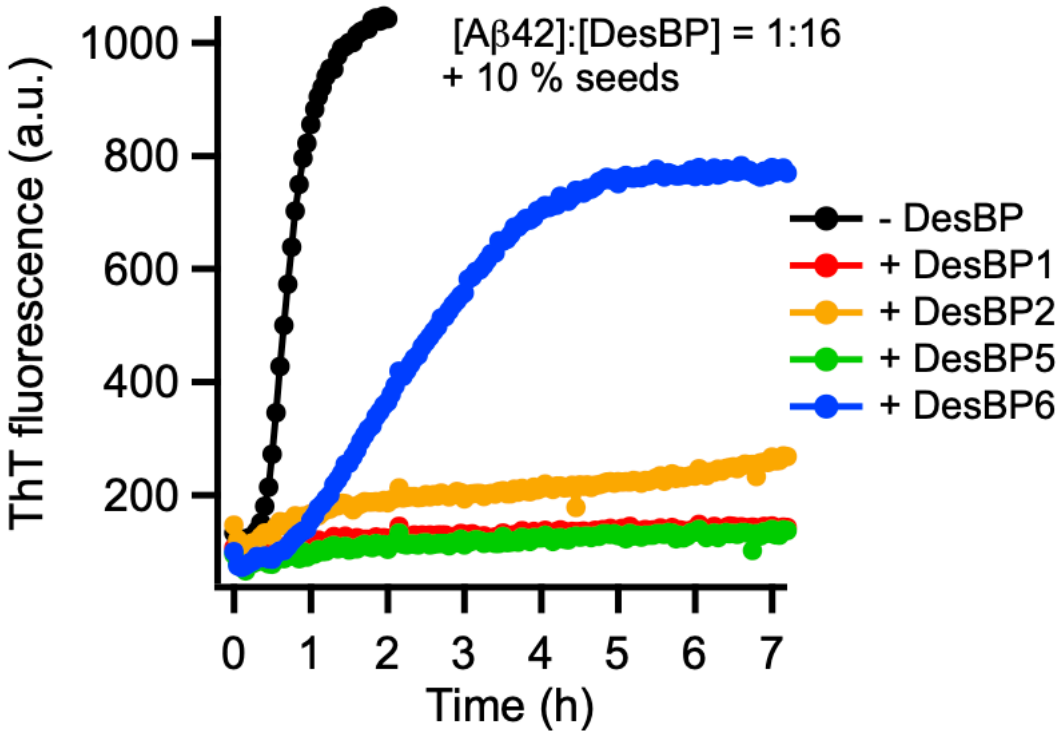

Figure S5. Seeded aggregation assay of Aβ42 in the presence of high molar equivalents of DesBPs. The aggregates formed in the presence of the DesBPs, with the exception of the case of DesBP6, did not show seeding ability indicating that they do not have a fibrillar nature. Experiments were performed in triplicate.

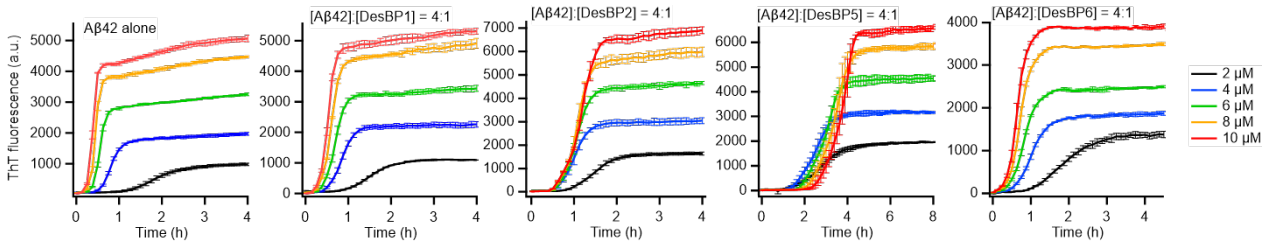

Figure S6. Kinetics of Aβ42 aggregation in the presence of 0.25 molar equivalents DesBPs. We report the results for increasing concentrations of Aβ42, from 2 to 10 μM. All experiments were performed in triplicate.